Element Selective Probe of the Ultra-Fast Magnetic Response to an Element Selective Excitation in Fe-Ni Compounds Using a Two-Color FEL Source

Eugenio Ferrari, Carlo Spezzani, Franck Fortuna, Renaud Delaunay, Franck Vidal, Ivaylo Nikolov, Paolo Cinquegrana, Bruno Diviacco, David Gauthier, Giuseppe Penco, et al.

photonics

MDPI

Article

Element Selective Probe of the Ultra-Fast Magnetic Response to an Element Selective Excitation in Fe-Ni Compounds Using a Two-Color FEL Source

Eugenio Ferrari [1,2,†], Carlo Spezzani [1,3], Franck Fortuna [4], Renaud Delaunay [5], Franck Vidal [6], Ivaylo Nikolov [1], Paolo Cinquegrana [1], Bruno Diviacco [1], David Gauthier [1], Giuseppe Penco [1], Primož Rebernik Ribič [1], Eléonore Roussel [1], Mauro Trovò [1], Jean-Baptiste Moussy [7], Tommaso Pincelli [8], Lounès Lounis [6,9], Cristian Svetina [1,10], Marco Zangrando [1,11], Nicola Mahne [1], Lorenzo Raimondi [1], Michele Manfredda [1], Emanuele Pedersoli [1], Flavio Capotondi [1], Alexander Demidovich [1], Luca Giannessi [1,12], Maya Kiskinova [1], Giovanni De Ninno [1,13], Miltcho Boyanov Danailov [1], Enrico Allaria [1,*] and Maurizio Sacchi [6,14,*]

1 ELETTRA—Sincrotrone Trieste, Area Science Park, 34149 Trieste, Italy; eugenio.ferrari@psi.ch (E.F.); carlo.spezzani@elettra.eu (C.S.); ivaylo.nikolov@elettra.eu (I.N.); paolo.cinquegrana@elettra.eu (P.C.); bruno.diviacco@elettra.eu (B.D.); david.gauthier@elettra.eu (D.G.); giuseppe.penco@elettra.eu (G.P.); primoz.rebernik@elettra.eu (P.R.R.); eleonore.roussel@elettra.eu (E.R.); mauro.trovo@elettra.eu (M.T.); Cristian.Svetina@elettra.eu (C.S.); Marco.Zangrando@elettra.eu (M.Z.); Nicola.Mahne@elettra.eu (N.M.); Lorenzo.Raimondi@elettra.eu (L.R.); michele.manfredda@elettra.eu (M.M.); emanuele.pedersoli@elettra.eu (E.P.); flavio.capotondi@elettra.eu (F.C.); alexander.demidovich@elettra.eu (A.D.); lucagiannessi@gmail.com (L.G.); maya.kiskinova@elettra.eu (M.K.); giovanni.deninno@elettra.eu (G.D.N.); miltcho.danailov@elettra.eu (M.B.D.)

2 Dipartimento di Fisica, Università degli Studi di Trieste, 34127 Trieste, Italy

3 Laboratoire de Physique des Solides, Université Paris-Sud, CNRS-UMR 8502, Bât. 510, 91405 Orsay, France

4 Centre de Sciences Nucléaires et de Sciences de la Matière, Université Paris-Sud, CNRS UMR 8609, Bât. 104-108, 91405 Orsay, France; fortuna@csnsm.in2p3.fr

5 Laboratoire de Chimie Physique Matière et Rayonnement, Sorbonne Universités, UPMC Univ Paris 06, CNRS UMR 7614, 75005 Paris, France; renaud.delaunay@upmc.fr

6 Institut des NanoSciences de Paris, Sorbonne Universités, UPMC Univ Paris 06, CNRS UMR 7588, 75005 Paris, France; franck.vidal@insp.jussieu.fr (F.V.); lounis@insp.jussieu.fr (L.L.)

7 Service de Physique de l'Etat Condensé, DSM/IRAMIS/SPEC, CNRS UMR 3680, CEA Saclay, 91191 Gif-sur-Yvette, France; jean-baptiste.moussy@cea.fr

8 Dipartimento di Fisica, Università degli Studi di Milano, 20133 Milano, Italy; tommaso.pincelli@gmail.com

9 Ecole Normale Supérieure, PSL Research University, 75231 Paris, France

10 Graduate School of Nanotechnology, Università degli Studi di Trieste, 34127 Trieste, Italy

11 Istituto Officina dei Materiali, Consiglio Nazionale delle Ricerche, 34149 Trieste, Italy

12 ENEA, Centro Ricerche Frascati, Via E. Fermi 45, 00044 Frascati, Italy

13 Laboratory of Quantum Optics, University of Nova Gorica, 5001 Nova Gorica, Slovenia

14 Synchrotron SOLEIL, L'Orme des Merisiers, Saint-Aubin, B.P. 48, 91192 Gif-sur-Yvette, France

* Correspondence: enrico.allaria@elettra.eu (E.A.); maurizio.sacchi@synchrotron-soleil.fr (M.S.)

† Current Address: Particle Accelerator Physics Laboratory, École Polytechnique Fédérale de Lausanne, 1015 Lausanne, Switzerland.

Received: 18 December 2016; Accepted: 20 January 2017; Published: 26 January 2017

Abstract: The potential of the two-color mode implemented at the FERMI free-electron laser (FEL) source for pumping and probing selectively different atomic species has been demonstrated by time-resolved scattering experiments with permalloy (FeNi alloy) and $NiFe_2O_4$ samples. We monitored the ultra-fast demagnetization of Ni induced by the pump FEL pulse, by tuning the linearly-polarized FEL probe pulse to the Ni-3p resonance and measuring the scattered intensity in the transverse magneto-optical Kerr effect geometry. The measurements were performed by varying the intensity of the FEL pump pulse, tuning its wavelength to and off of the Fe-3p resonance, and by spanning the FEL probe pulse delays across the 300–900 fs range. The obtained results have

evidenced that for the case of $NiFe_2O_4$, there is a sensible difference in the magnetic response at the Ni site when the pump pulse causes electronic excitations at the Fe site.

Keywords: free electron laser; two-color source; ultra-fast dynamics

1. Introduction

The most common approach to ultra-fast demagnetization relies on optical-laser based time-resolved magneto-optical Kerr effect (MOKE) studies [1,2]. Modern pulsed X-ray sources, notably free-electron lasers (FEL) and high-harmonic generation sources, have introduced the use of X-rays as a complement to optical lasers. The most common set-up makes use of an optical laser as the pump and of an X-ray beam as the probe, providing element selectivity by fine-tuning the X-ray wavelength to a core resonance [3–6]. We developed a new scheme where, in a given multi-element magnetic sample, we pump one selected element and probe another element, also selectively, using two FEL pulses of different wavelengths [7]. The interest of this kind of experiment resides in the possibility of associating the pump energy with a specific electronic excitation of one component of a complex system. The combination of an element selective excitation with an element selective probe offers new paths for unraveling the fundamental mechanisms that drive magnetization loss by separately addressing the weight of possible contributions in this complex problem. Important classes of magnetic materials, in this respect, are ferrites [8,9] and transition metal (TM) rare-earth (RE) compounds [10–13]. Beyond their applicative interest, the (O-mediated) TM-TM coupling in magnetic oxides and the (5d-mediated) 3d-4f coupling in TM-RE compounds make these materials ideal candidates for resonant-pump resonant-probe magnetization dynamics studies. The highly localized 3d and 4f orbitals and the mediated coupling make it plausible that associating the pump energy with a specific electronic excitation can influence the magnetization dynamics profoundly, compared to using a non-resonant pump.

2. Materials and Methods

2.1. Source Design

The conceptual and experimental development of two-color schemes prompted major research efforts at all FEL facilities worldwide [14–18], with the ambition of optimizing wavelength and timing control. In general, two-color sources are constrained by limited wavelength tunability. Recently, a new configuration of the FERMI FEL-1 seeded source [19] was implemented that delivers two time-delayed FEL pulses with different wavelengths, each independently tunable over a broad spectral range. The principle of the two-color double-resonant source was set out in reference [7]. Here we summarize its most relevant features.

The twin-seed layout starts from a common ~780 nm laser source that produces two ultraviolet (UV) pulses along two distinct optical paths. One comprises a third-harmonic generator and a delay-line for adjusting the delay Δt between the two pulses. The other features an optical parametric amplifier (OPA) for adjusting the pulse wavelength over the 230–260 nm range. The former, which has a fixed 261.5 nm wavelength and a FWHM pulse duration t_{seed} of ~120 fs, serves as a UV seed for producing the Ni-3p resonant FEL pulse. The latter, with t_{seed} ~150 fs, is used for seeding the Fe-3p resonant FEL emission by setting its wavelength to 255 nm. The two UV seeds are recombined and kept along the same optical path by using a feed-back system based on multiple motorized piezoelectric tip-tilt devices.

Figure 1 sketches the principle of the two-color resonant FEL mode used in our experiment. The two UV laser seeds are aligned with the electron beam trajectory within the FEL modulator section, where they interact with the electron bunch, stretched in time to ~1 ps length. The wavelength

separation between the two seeds is smaller than the bandwidth accepted by the modulator (~3%), but larger than that accepted by the radiator (~0.7%). The FERMI FEL-1 radiator section is composed of six undulator modules. For most of the measurements, five modules (Rad_2 in Figure 1a) are tuned to the 11th harmonic of the 255 nm seed laser, generating a FEL pump pulse at 23.2 nm (53.5 eV), i.e., at the Fe-3p resonance (Figure 1a). By controlling the seed laser intensity via cross-polarizers, the energy per FEL pulse spans the 0 to 10 μJ range, corresponding to a pump fluence (F) of 0–40 mJ·cm^{-2} at the sample position. Off-resonance pumping (Figure 1b) is obtained by tuning Rad_2 to the 10th harmonic, corresponding to 25.5 nm (48.6 eV). The remaining radiator module (Rad_1) is tuned to the 14th harmonic of the 261.5 nm seed pulse, resulting in a FEL emission at 18.6 nm (67 eV, Ni-3p resonance), with a maximum energy of ~0.8 μJ per pulse. We also tested a different source scheme with inverted pump and probe wavelengths and an equal distribution of the radiator modules on the Rad_1 and Rad_2 sub-sections (Figure 1c). The delay Δt between the two UV seeds, measured by a cross-correlator, can be adjusted over the 300–900 fs range with negligible (<5 fs) jitter [20,21]. The upper limit is imposed by the electron bunch length of ~1 ps. Cross-talk and instabilities are observed in the double FEL emission below 300 fs separation, hampering the collection of reliable data at shorter delays. The duration t_{FEL} of each FEL pulse can be conservatively estimated from t_{seed} by the scaling law $t_{FEL} = t_{seed} \times h^{-0.3}$, h being the radiator harmonic. Therefore the FEL pulses in our experiment are expected to have a 50 to 70 fs duration, for an overall time resolution better than 100 fs.

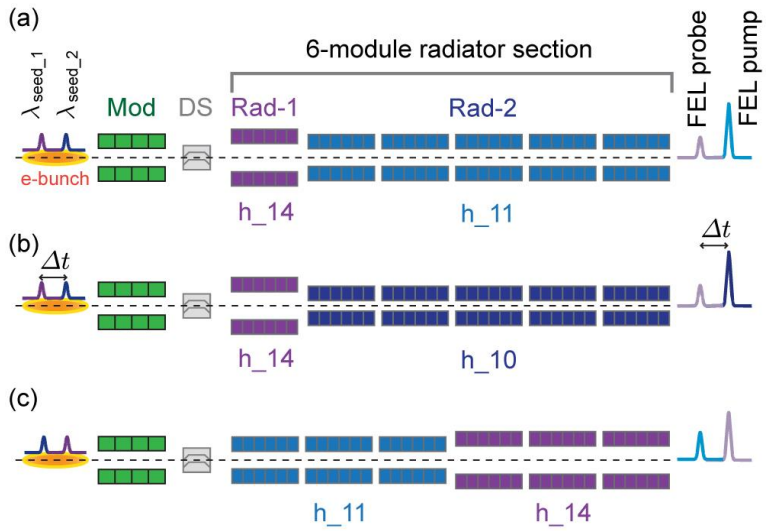

Figure 1. Twin-seed split-radiator source scheme. (**a**) Ni-3p resonant probe, Fe-3p resonant pump. The two UV seed pulses, controlled in intensity and separated by a well-defined time delay Δt, interact with the electron bunch within the modulator (Mod) section. After going through the dispersive section (DS), the electron excitation induced by the probe seed pulse (λ_{seed_1} = 261.5 nm) is amplified by the first of the six radiator modules (Rad_1) tuned to harmonic 14 (h_14), generating 18.6 nm free-electron laser (FEL) radiation (67 eV, Ni-3p resonance). This excitation is not amplified by the five other radiator modules (Rad_2). Conversely, the UV pump seed (λ_{seed_2} = 255 nm) induces an excitation of the electron bunch that is amplified by tuning Rad_2 to the 11th harmonic, generating a 23.2 nm FEL pulse (53.5 eV, Fe-3p resonance), but this excitation is not amplified by Rad_1. The source delivers two FEL pulses tuned in energy to the Fe-3p and Ni-3p resonances, with controlled intensities and time separation; (**b**) Ni-3p resonant probe, non-resonant pump. The same seeding scheme as in (**a**) applies, but the Rad_2 radiator sub-section is tuned to h_10 of the 255 nm pump seed, generating 25.5 nm FEL radiation, whose photon energy is insufficient to photo-excite the core electrons of either Fe or Ni; (**c**) Fe-3p resonant probe, Ni-3p resonant pump. The wavelengths of the two UV seeds are inverted (λ_{seed_1} = 255 nm, λ_{seed_2} = 261.5 nm) and the radiator is split in two sub-sections of three modules each. Rad_1 provides the 23.3 nm FEL probe pulse tuned to the Fe-3p resonance, while Rad_2 generates the Ni-3p resonant 18.6 nm pump pulse.

2.2. Experimental Details

The measurements were performed at the DiProI beamline [22,23] of the FERMI FEL source, using the IRMA (Instrument pour la Réfléctivité MAgnétique) scattering chamber [24]. Figure 2 shows a sketch of the experimental set-up and of the data collection method. After aligning the sample using the two-axis goniometer, the pump-probe results were monitored using a charge-coupled device (CCD) detector. The grating-like structure of the samples separated the pump and probe contributions spatially, allowing us to discriminate the diffracted intensities at the two wavelengths. The diffraction peaks corresponding to the pump and probe FEL wavelengths were collected simultaneously on the CCD. Blanking out one of the FEL beams allowed us to check for cross-talking between them. We confirmed its absence for delays exceeding 300 fs, while interference between the two sources was observed at shorter delays. In order to maximize the magnetic signal, we worked in transverse-MOKE geometry [25,26], setting the incidence angle to 46.5°, i.e., close to the Brewster angle. We used linear vertical polarization of the FEL pulses, taking advantage of the Apple-II undulators in the FERMI radiator [27].

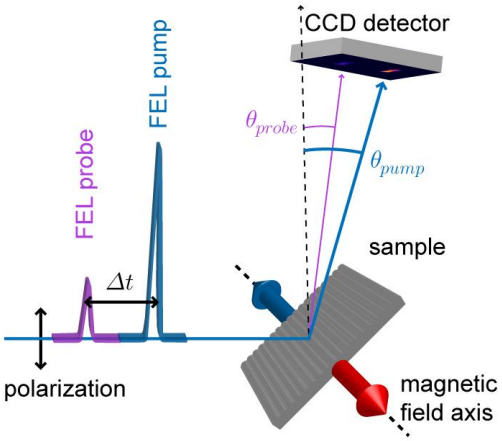

Figure 2. Schematics of the scattering measurement setup. The grating samples are mounted in a reflectometer featuring a vertical scattering plane. A magnetic field (up to 1.5 kOe pulsed, 500 Oe permanent) can be applied normal to the scattering plane and parallel to the sample surface by a horseshoe electromagnet. The FEL pulses with linear vertical polarization impinge on the sample grating at 46.5° and are diffracted at different angles according to their wavelengths. Diffracted intensities from the pump and probe FEL pulses are collected simultaneously by using a two-dimensional charge-coupled device detector.

We measured two samples. The first is a 20 nm permalloy (Py) film, deposited on a 605 nm period Si grating and protected by a 3 nm Al capping layer (Figure 3a, FEL data). Its magnetic properties were characterized by MOKE using an optical laser (Figure 3b). The second is a 12.5 nm thick Ni-ferrite ($NiFe_2O_4$) layer grown epitaxially on $MgAl_2O_4$(001) [28]. A 100 × 400 μm^2 area of the layer was ruled by focused ion beam (FIB) etching into a set of ~350 nm wide stripes with a ~600 nm period (Figure 3c). Magnetization curves showed a coercive field of ~500 Oe with >80% remanence (Figure 3d, FEL data). It is worth stressing that the fraction of pump energy absorbed in the Ni-ferrite sample is the same (~78% for the 12.5 nm thick film at 46.5° incidence) for both resonant (22.3 nm) and non-resonant (25.5 nm) pump wavelengths.

The Ni magnetic signal at different pump-probe delays was measured as a function of the pump fluence F, for both Fe-3p resonant and non-resonant pump wavelengths, using the acquisition procedure sketched in Figure 4.

A reliable analysis of the demagnetization in a pump-probe experiment requires the sample to be homogeneously pumped over the probed area. From the images in Figures 4 and 5, it is apparent that

this is not the case if one integrates the scattered probe signal over the entire diffraction spot, since both the pump and the probe have an inhomogeneous spatial distribution of the intensity. In order to avoid averaging the probe signal over areas that are pumped differently, the magnetic signal reported in the following corresponds to the probe intensity scattered within a detector portion of 7 × 7 pixels (Figure 5) that measures the homogeneously pumped area.

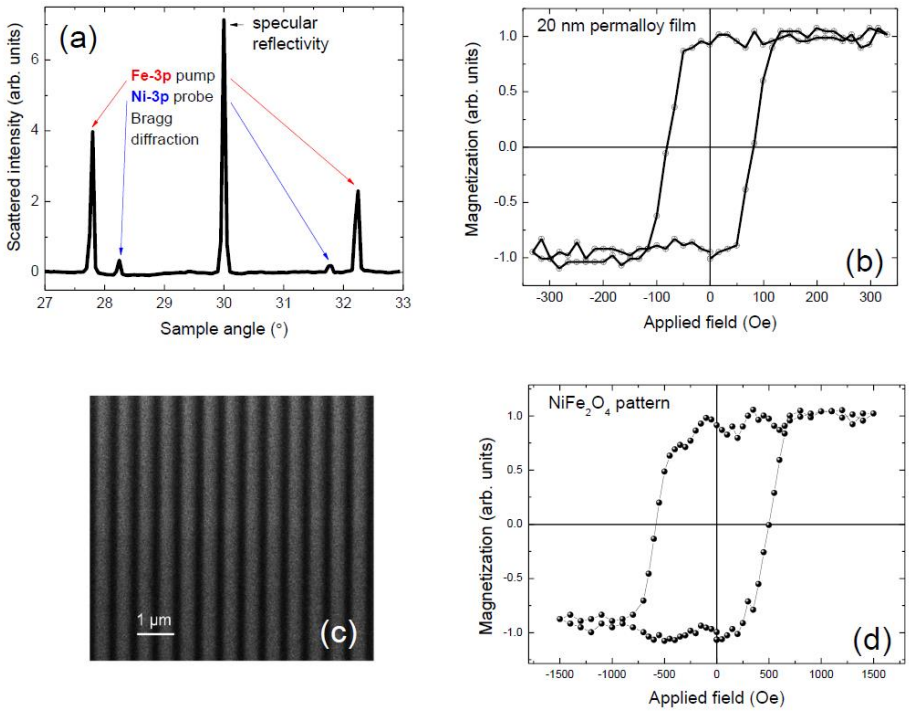

Figure 3. Permalloy and Ni-ferrite samples. (**a**) Rocking scan of the Py grating sample, showing the Bragg peaks corresponding to the Fe-3p resonant pump and to the Ni-3p resonant probe FEL beams; (**b**) Hysteresis loop of the Py magnetization measured by magneto-optical Kerr effect (MOKE), with the magnetic field applied parallel to the grating lines; (**c**) Scanning electron microscopy image of the Ni-ferrite sample. An area of 100 × 400 μm^2 is patterned into a ~600 nm period grating by focused ion beam etching; (**d**) Field dependence of the FEL radiation intensity diffracted at the Fe-3p resonance, measuring the magnetic response over the ruled area of the Ni-ferrite.

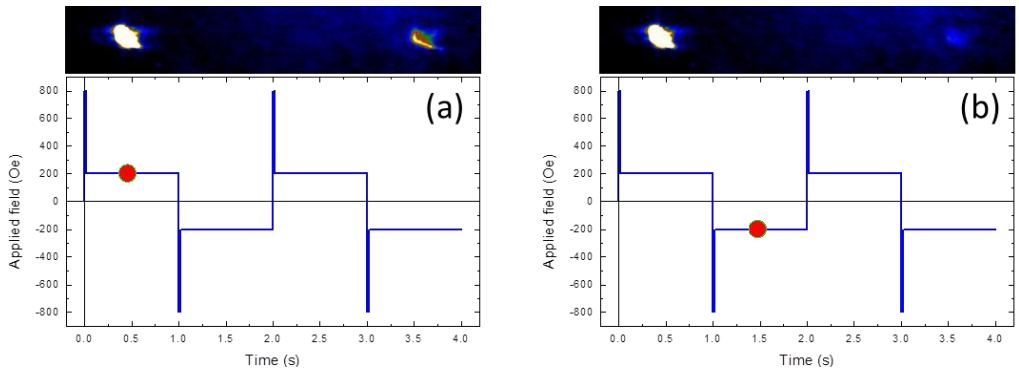

Figure 4. Data acquisition sequence. Sketch of the acquisition sequence used for determining the magnetic signal. (**a**) After a +800 Oe pulse of ~10 ms duration, data are collected in a +200 Oe applied field; (**b**) Same as (**a**), for negative field values. The magnetic signal is defined as the difference divided by the sum of the signals measured for opposite magnetization directions. Top panels: CCD images of the pump (left spot) and probe (right spot) scattered intensities.

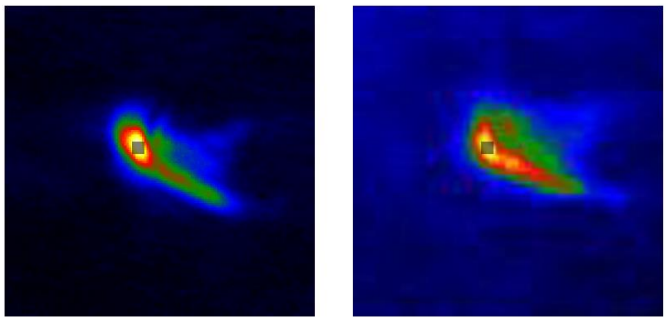

Figure 5. Measurement area selection. Fe-3p resonant pump (**a**) and Ni-3p resonant probe (**b**) diffracted intensity from the Ni-ferrite sample. The two images are shown on different color scales. The gray square represents the 7 × 7 pixels area used for Ni-magnetization analysis, where the pump fluence is assumed to be homogeneous.

3. Results

Figure 6 shows the dependence of the Ni magnetic signal on the pump fluence at a probe delay of 420 fs in Py. The pump fluence at the sample (F, top scale in Figure 6, in mJ·cm^{-2}) is obtained by correcting the pump energy measured at the exit of the FEL source (bottom scale in Figure 6, in μJ) for the transport line transmission (a factor of 0.4, accounting for six reflections and a 200 nm Al filter), for the focal spot size (~80 μm), and for the angle of incidence (46.5°). The Ni magnetic signal is the asymmetry ratio in the Bragg peak intensity, i.e., the difference between the scattered intensities for opposite signs of the saturation magnetization direction, divided by their sum (see Figure 4). Figure 6 shows the loss in Ni magnetic signal with respect to the static value measured without the pump. The red and blue dots refer to the Fe-3p resonant (23.2 nm) and non-resonant (25.5 nm) pumping, respectively. The results do not evidence any clear dependence on the pump wavelength; both curves show the same trend of the Ni demagnetization with F, attaining a ~50% reduction at 10 mJ·cm^{-2}.

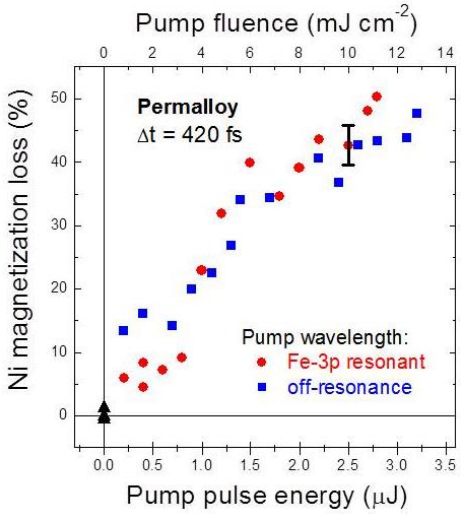

Figure 6. Ni magnetic response in permalloy. F dependence of the Ni magnetization loss in Py, 420 fs after the pump pulse. The red circles and blue squares refer to 53.5 eV Fe-3p resonant and to 48.6 eV non-resonant pump pulses, respectively. The pump fluence at the sample (top scale) is estimated from the pump intensity measured at the exit of the source (bottom scale). The Ni magnetization loss represents the decrease in the asymmetry ratio signal at the Bragg peak with respect to the non-pumped condition (black triangles). The black vertical bar corresponds to one standard deviation in the value of the measured magnetic signal.

The same experiment was performed with the $NiFe_2O_4$ sample. First, we verified that the epitaxial oxide layer on a low thermal conductivity insulating substrate could stand our pump-probe conditions. Then we checked that the chosen 12.5 nm thickness, ensuring homogeneous absorption of the pump energy, provided a convenient magnetic signal in the diffracted intensity. We found that inverting the saturation magnetization direction provides an excellent 80% asymmetry ratio at Ni-3p resonance.

Figure 7a shows the Ni magnetization loss after 400 fs as a function of F. There is a clear difference between the data obtained using a non-resonant (blue dots) and an Fe-3p resonant (red dots) pump pulse, showing the influence of the pump wavelength on the Ni demagnetization. This sensitivity of the Ni-ferrite sample to the Fe-3p resonant and off-resonant pumping is also confirmed by the results obtained as a function of the pump-probe delay reported in Figure 7b,c. Dependence on the pump wavelength is observed already at the lower fluence F = 4 mJ·cm^{-2} (Figure 7b), and it becomes much more evident and well beyond experimental uncertainty at F = 10 mJ·cm^{-2} (Figure 7c). Figure 7b,c shows that for both F values, the quenching of the Ni magnetization is initially rather slow and reaches a maximum after ~500 fs.

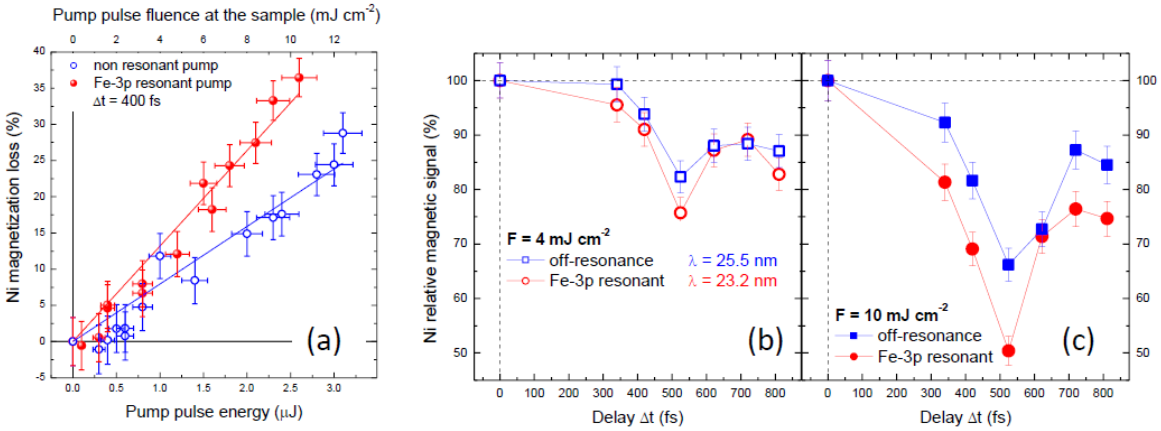

Figure 7. Ni magnetic response in Ni-ferrite. (**a**) Relative Ni magnetization loss as a function of F for Fe-3p resonant and non-resonant pumping, at a fixed delay of 400 fs; (**b**,**c**) Normalized Ni magnetization as a function of delay Δt for resonant and non-resonant pumping at F = 4 mJ·cm^{-2} (**b**) and F = 10 mJ·cm^{-2} (**c**). Error bars on Δt ($\pm$5 fs) are smaller than the symbol size.

4. Conclusions and Outlook

The observed different demagnetization behavior of the two Fe-Ni compounds under investigation can be qualitatively ascribed to the fundamental differences in their electronic structures. Permalloy is a ferromagnetic metallic alloy where Fe-3d and Ni-3d electrons, which determine the magnetic properties, pertain to strongly hybridized and delocalized orbitals featuring direct exchange. In the ferrimagnetic oxide $NiFe_2O_4$, the 3d electrons are much more localized onto the respective atomic sites and the exchange is mainly mediated by oxygen. Releasing the pump energy to the ensemble of the 3d electrons (off-resonant pumping) or more selectively to the Fe site via 3p-3d core excitations (Fe-3p resonant pumping) is likely to make a difference in the Ni magnetic response when the 3d electrons are localized and interact via an indirect exchange, as it is the case for the Ni-ferrite. Our results show that the resonant/non-resonant character of the pump affects the degree of magnetization loss but not its delay dependence. Since no experimental or theoretical studies have addressed this kind of problem yet, we are not in a condition of interpreting this result at a more fundamental level.

The two-color mode developed at FERMI provides a versatile source of FEL twin-pulses with controlled wavelength tunability and time separation. The use of two optical laser seeds allows for the fast and independent control of the intensity and time separation of the two FEL pulses. Additionally, the inversion of the pump and probe wavelengths can be performed in a reasonable

time lapse: the reconfiguration of the radiator modules for probing the Fe magnetic signal while pumping the Ni resonantly (Figure 8) took less than one hour. The red circles in Figure 8 represent the Fe demagnetization in the Ni-ferrite as a function of the Ni-3p resonant pump fluence. The blue circles represent the Fe-3p resonant probe fluence, showing that it is not affected by varying the Ni-resonant pump intensity over the same *F* range.

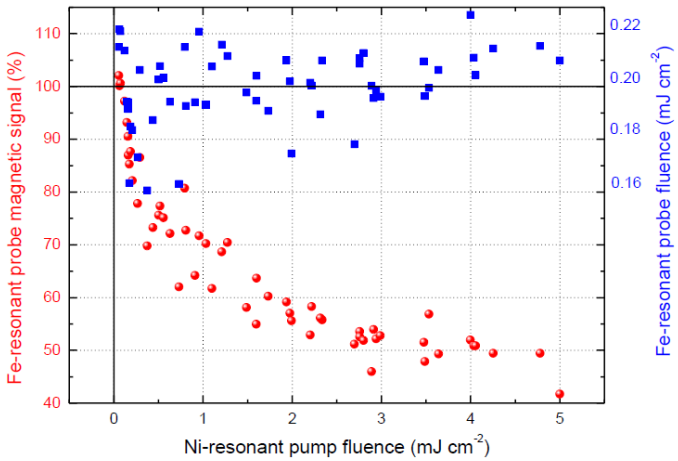

Figure 8. Ni-3p pump/Fe-3p probe resonant magnetic scattering in $NiFe_2O_4$. The Fe magnetic signal is measured 530 fs after the pump pulse as a function of the pump fluence (red circles, left axis). The Fe-resonant probe fluence (blue squares, right axis) is unaffected over the spanned range of pump fluence.

Our first results with two magnetic compounds containing Fe and Ni illustrate the potential of the on/off resonance FEL pump-probe experiments. In its present version, the twin-seeded two-color FEL source at FERMI can cover the 3p resonances of Mn, Fe, Co, and Ni, making a wide class of important magnetic materials accessible for time resolved experiments. We stress that this kind of source can find original applications well beyond ultrafast demagnetization studies, in many other fields of condensed matter and of atomic and molecular physics. In general, it enables the excitation of a core resonance on a specific atomic site in a complex system with pulses of selected wavelength, intensity, and polarization, and makes it possible to probe the dynamic response at another atomic site with a second FEL pulse. Such multi-colour time-resolved experiments open unique opportunities for exploring complex relaxation processes, such as sequential multiple ionizations, multi-electron cascades, and charge transfer dynamics.

Acknowledgments: We are grateful to Jan Vogel (Institut Néel, Grenoble), Giancarlo Panaccione (CNR-IOM, Trieste), Fausto Sirotti (Synchrotron SOLEIL), Nicolas Moisan (LPS, Orsay), Michael Meyer (European XFEL, Hamburg), and Coryn F. Hague (LCPMR, Paris) for useful discussions and suggestions. This research received financial support from the European Community 7th Framework Programme under grant agreement No. 312284, and from CNRS (France) via the PEPS_SASLELX program. The FERMI project at Elettra—Sincrotrone Trieste is supported by MIUR under grants FIRB-RBAP045JF2 and FIRB-RBAP06AWK3.

Author Contributions: E.F., C. Spezzani, G.D.N., M.B.D., E.A., and M.S. conceived and coordinated the experiment. E.F., C. Spezzani, L.G., G.D.N., M.B.D., and E.A. designed the two-colour scheme. I.N., P.C., A.D., and M.B.D. operated the laser source. E.F., B.D., D.G., G.P., P.R.R., E.R., M.T., L.G., G.D.N., and E.A. operated the F.E.L. source. F.F., R.D., F.V., J.-B.M., and L.L. fabricated and characterized the samples. C. Svetina, M.Z., N.M., L.R., M.M., E.P., F.C., and M.K. contributed to the DIPROI setup. C. Spezzani, F.F., R.D., T.P., and M.S. prepared and performed the scattering experiment. E.F., C. Spezzani, F.V., M.K., G.D.N., M.B.D., E.A., and M.S. analysed the data and wrote the manuscript, with contributions from all authors.

Conflicts of Interest: The authors declare no conflict of interest.

References

1. Beaurepaire, E.; Merle, J.-C.; Daunois, A.; Bigot, J.-Y. Ultrafast spin dynamics in ferromagnetic nickel. *Phys. Rev. Lett.* **1996**, *76*, 4250. [CrossRef] [PubMed]
2. Koopmans, B.; Malinowski, G.; Dalla Longa, F.; Steiauf, D.; Fahnle, M.; Roth, T.; Cinchetti, M.; Aeschlimann, M. Explaining the paradoxical diversity of ultrafast laser-induced demagnetization. *Nat. Mater.* **2010**, *9*, 259–265. [CrossRef] [PubMed]
3. Stamm, C.; Kachel, T.; Pontius, N.; Mitzner, R.; Quast, T.; Holldack, K.; Khan, S.; Lupulescu, C.; Aziz, E.F.; Wietstruk, M.; et al. Femtosecond modification of electron localization and transfer of angular momentum in nickel. *Nat. Mater.* **2007**, *6*, 740–743. [CrossRef] [PubMed]
4. Boeglin, C.; Beaurepaire, E.; Halte, V.; Lopez-Flores, V.; Stamm, C.; Pontius, N.; Durr, H.A.; Bigot, J.-Y. Distinguishing the ultrafast dynamics of spin and orbital moments in solids. *Nature* **2010**, *465*, 458–461. [CrossRef] [PubMed]
5. Pontius, N.; Kachel, T.; Schüßler-Langeheine, C.; Schlotter, W.F.; Beye, M.; Sorgenfrei, F.; Chang, C.F.; Föhlisch, A.; Wurth, W.; Metcalf, P.; et al. Time-resolved resonant soft X-ray diffraction with free-electron lasers: Femtosecond dynamics across the Verwey transition in magnetite. *Appl. Phys. Lett.* **2011**, *98*, 182504. [CrossRef]
6. Eschenlohr, A.; Battiato, M.; Maldonado, P.; Pontius, N.; Kachel, T.; Holldack, K.; Mitzner, R.; Föhlisch, A.; Oppeneer, P.M.; Stamm, C. Ultrafast spin transport as key to femtosecond demagnetization. *Nat. Mater.* **2013**, *12*, 332–336. [CrossRef] [PubMed]
7. Ferrari, E.; Spezzani, C.; Fortuna, F.; Delaunay, R.; Vidal, F.; Nikolov, I.; Cinquegrana, P.; Diviacco, B.; Gauthier, D.; Penco, G.; et al. Widely tunable two-colour seeded free-electron laser source for resonant-pump resonant-probe magnetic scattering. *Nat. Commun.* **2016**, *7*, 10343. [CrossRef] [PubMed]
8. Muller, G.M.; Walowski, J.; Djordjevic, M.; Miao, G.X.; Gupta, A.; Ramos, A.V.; Gehrke, K.; Moshnyaga, V.; Samwer, K.; Schmalhorst, J.; et al. Spin polarization in half-metals probed by femtosecond spin excitation. *Nat. Mater.* **2009**, *8*, 56–61. [CrossRef] [PubMed]
9. Först, M.; Caviglia, A.D.; Scherwitzl, R.; Mankowsky, R.; Zubko, P.; Khanna, V.; Bromberger, H.; Wilkins, S.B.; Chuang, Y.-D.; Lee, W.S.; et al. Spatially resolved ultrafast magnetic dynamics initiated at a complex oxide heterointerface. *Nat. Mater.* **2015**, *14*, 883–888. [CrossRef] [PubMed]
10. Wietstruk, M.; Melnikov, A.; Stamm, C.; Kachel, T.; Pontius, N.; Sultan, M.; Gahl, C.; Weinelt, M.; Dürr, H.A.; Bovensiepen, U. Hot-electron-driven enhancement of spin-lattice coupling in Gd and Tb 4f ferromagnets observed by femtosecond X-ray magnetic circular dichroism. *Phys. Rev. Lett.* **2011**, *106*, 127401. [CrossRef] [PubMed]
11. Radu, I.; Vahaplar, K.; Stamm, C.; Kachel, T.; Pontius, N.; Durr, H.A.; Ostler, T.A.; Barker, J.; Evans, R.F.L.; Chantrell, R.W.; et al. Transient ferromagnetic-like state mediating ultrafast reversal of antiferromagnetically coupled spins. *Nature* **2011**, *472*, 205–208. [CrossRef] [PubMed]
12. Graves, C.E.; Reid, A.H.; Wang, T.; Wu, B.; de Jong, S.; Vahaplar, K.; Radu, I.; Bernstein, D.P.; Messerschmidt, M.; Müller, L.; et al. Nanoscale spin reversal by non-local angular momentum transfer following ultrafast laser excitation in ferrimagnetic GdFeCo. *Nat. Mater.* **2013**, *12*, 293–298. [CrossRef] [PubMed]
13. Le Guyader, L.; Savoini, M.; El Moussaoui, S.; Buzzi, M.; Tsukamoto, A.; Itoh, A.; Kirilyuk, A.; Rasing, T.; Kimel, A.V.; Nolting, F. Nanoscale sub-100 picosecond all-optical magnetization switching in GdFeCo microstructures. *Nat. Commun.* **2015**, *6*, 5839. [CrossRef] [PubMed]
14. Allaria, E.; Bencivenga, F.; Borghes, R.; Capotondi, F.; Castronovo, D.; Charalambous, P.; Cinquegrana, P.; Danailov, M.B.; de Ninno, G.; Demidovich, A.; et al. Two-colour pump–probe experiments with a twin-pulse-seed extreme ultraviolet free-electron laser. *Nat. Commun.* **2013**, *4*, 2476. [CrossRef] [PubMed]
15. Hara, T.; Inubushi, Y.; Katayama, T.; Sato, T.; Tanaka, H.; Tanaka, T.; Togashi, T.; Togawa, K.; Tono, K.; Yabashi, M.; et al. Two-colour hard X-ray free-electron laser with wide tunability. *Nat. Commun.* **2013**, *4*, 2919. [CrossRef] [PubMed]
16. Lutman, A.A.; Decker, F.-J.; Arthur, J.; Chollet, M.; Feng, Y.; Hastings, J.; Huang, Z.; Lemke, H.; Nuhn, H.-D.; Marinelli, A.; et al. Demonstration of single-crystal self-seeded two-color X-ray free-electron lasers. *Phys. Rev. Lett.* **2014**, *113*, 254801. [CrossRef] [PubMed]

17. Marinelli, A.; Ratner, D.; Lutman, A.A.; Turner, J.; Welch, J.; Decker, F.J.; Loos, H.; Behrens, C.; Gilevich, S.; Miahnahri, A.A.; et al. High-intensity double-pulse X-ray free-electron laser. *Nat. Commun.* **2015**, *6*, 6369. [CrossRef] [PubMed]
18. Lutman, A.A.; Maxwell, T.J.; MacArthur, J.P.; Guetg, M.W.; Berrah, N.; Coffee, R.N.; Ding, Y.; Huang, Z.; Marinelli, A.; Moeller, S.; et al. Fresh-slice multicolour X-ray free-electron lasers. *Nat. Photonics* **2016**, *10*, 745–750. [CrossRef]
19. Allaria, E.; Appio, R.; Badano, L.; Barletta, W.A.; Bassanese, S.; Biedron, S.G.; Borga, A.; Busetto, E.; Castronovo, D.; Cinquegrana, P.; et al. Highly coherent and stable pulses from the FERMI seeded free-electron laser in the extreme ultraviolet. *Nat. Photon.* **2012**, *6*, 699–704. [CrossRef]
20. Danailov, M.B.; Bencivenga, F.; Capotondi, F.; Casolari, F.; Cinquegrana, P.; Demidovich, A.; Giangrisostomi, E.; Kiskinova, M.P.; Kurdi, G.; Manfredda, M.; et al. Towards jitter-free pump-probe measurements at seeded free electron laser facilities. *Opt. Express* **2014**, *22*, 12869–12879. [CrossRef] [PubMed]
21. Cinquegrana, P.; Cleva, S.; Demidovich, A.; Gaio, G.; Ivanov, R.; Kurdi, G.; Nikolov, I.; Sigalotti, P.; Danailov, M.B. Optical beam transport to a remote location for low jitter pump-probe experiments with a free electron laser. *Phys. Rev. Spec. Top. Accel. Beams* **2014**, *17*, 040702. [CrossRef]
22. Pedersoli, E.; Capotondi, F.; Cocco, D.; Zangrando, M.; Kaulich, B.; Menk, R.H.; Locatelli, A.; Mentes, T.O.; Spezzani, C.; Sandrin, G.; et al. Multipurpose modular experimental station for the DiProI beamline of Fermi@Elettra free electron laser. *Rev. Sci. Instrum.* **2011**, *82*, 043711. [CrossRef] [PubMed]
23. Capotondi, F.; Pedersoli, E.; Mahne, N.; Menk, R.H.; Passos, G.; Raimondi, L.; Svetina, C.; Sandrin, G.; Zangrando, M.; Kiskinova, M.; et al. Invited Article: Coherent imaging using seeded free-electron laser pulses with variable polarization: First results and research opportunities. *Rev. Sci. Instrum.* **2013**, *84*, 051301. [CrossRef] [PubMed]
24. Sacchi, M.; Spezzani, C.; Torelli, P.; Avila, A.; Delaunay, R.; Hagie, C.F. Ultra-high vacuum soft X-ray reflectometer. *Rev. Sci. Instrum.* **2003**, *74*, 2791–2795. [CrossRef]
25. Spezzani, C.; Ferrari, E.; Allaria, E.; Vidal, F.; Ciavardini, A.; Delaunay, R.; Capotondi, F.; Pedersoli, E.; Coreno, M.; Svetina, C.; et al. Magnetization and microstructure dynamics in Fe/MnAs/GaAs(001): Fe magnetization reversal by a femtosecond laser pulse. *Phys. Rev. Lett.* **2014**, *113*, 247202. [CrossRef] [PubMed]
26. Sacchi, M.; Panaccione, G.; Vogel, J.; Mirone, A.; van der Laan, G. Magnetic dichroism in reflectivity and photoemission using linearly polarized light: 3*p* core level of Ni(110). *Phys. Rev. B* **1998**, *58*, 3750. [CrossRef]
27. Allaria, E.; Diviacco, B.; Callegari, C.; Finetti, P.; Mahieu, B.; Viefhaus, J.; Zangrando, M.; de Ninno, G.; Lambert, G.; Ferrari, E.; et al. Control of the polarization of a vacuum-ultraviolet, high-gain, free-electron laser. *Phys. Rev. X* **2014**, *4*, 041040. [CrossRef]
28. Matzen, S.; Moussy, J.-B.; Wei, P.; Gatel, C.; Cezar, J.C.; Arrio, M.A.; Sainctavit, P.; Moodera, J.S. Structure, magnetic ordering, and spin filtering efficiency of $NiFe_2O_4$(111) ultrathin films. *Appl. Phys. Lett.* **2014**, *104*, 182404. [CrossRef]